Chapter 2

MEASUREMENTS OF TOTAL PHOTON-ATOM AND PHOTOELECTRIC ABSORPTION CROSS SECTIONS NEAR PAIR PRODUCTION THRESHOLD

2.1. Introduction

The interaction of photons with matter represents one of the most varied classes of phenomena. A photon can interact with an atom in a number of ways. The most important interactions leading to the attenuation of a low-energy γ-ray beam are: (1) Rayleigh (coherent) scattering by bound atomic electrons, (2) Compton (incoherent) scattering by atomic electrons, (3) photoelectric absorption by atoms and (4) pair production in nuclear and (5) pair production in electron fields. Other interactions such as nuclear Thomson and nuclear resonance scattering by the nucleus, Delbrück scattering by the Coulomb field of the nucleus, double-Compton scattering and photonuclear reactions produce negligible effects at energies near the pair production threshold and below. The total photon cross section per atom σ_{tot} is, therefore, obtained by summing the cross sections for the processes (1) to (5)

$$\sigma_{tot} = \sigma_{coh} + \sigma_{incoh} + \tau + \kappa_n + \kappa_e , \qquad (2.1)$$

where σ_{coh}, σ_{incoh}, τ, κ_n and κ_e are the cross sections of the processes (1) to (5) respectively.

An extensive range of experiments on the measurement of γ-ray attenuation coefficients covering a wide range of photon-energies and for almost all the elements of periodic table, have been reported so far. For survey of experiments carried out till 1995 one can refer the bibliography of Hubbell *et al.* [117]. Not many experiments have been performed recently except for low-Z materials or at absorption edges.

Predictions of processes (1) to (5) have been summed up to prepare tabulations of attenuation coefficients for all elements and most of the photon energies. The tabulation prepared by Hubbell et al [118] is one of the most widely used data and it also provides references to most of the concerned theoretical works. The online databases such as XCOM [119, 120], XAAMDI [121] and FFAST [122], which are frequently used in current works relating to attenuation coefficients, are available in NIST (National Institute of Standards and Technology) website. The XCOM [119] provides total cross section of elements (Z=1 to 92) along with the cross sections of the individual processes (1) to (5) for photon energies ranging from 1 keV to 100 GeV. In XAAMDI one can also find attenuation coefficients of 48 compounds and mixtures of radiological interests besides those of elements for energies ranging from 1 keV to 20 MeV. The formalisms adopted in XCOM and XAAMDI are similar. The tabulations in FFAST include X-ray cross sections for energies through 2 to 433 keV. The theoretical and computational considerations adopted in FFAST are slightly different from those in XCOM, which can be seen [119, 120, 122].

The overall agreement between the predictions and the measurements of attenuation coefficients are good [117]. However, there exists some discrepancy between the XCOM and FFAST predictions for high Z elements. For Z lying between 60 and 82 the discrepancies being 15-50 % near absorption edges and 2-5 % throughout the high energy range [123]. The fractional difference, between the predictions of FFAST and

XCOM, in photoelectric cross sections varies between 2-5 % in the energy range 0.15-0.30 MeV for most of the elements. It is more (about 5-10 %) at the higher energies (0.3-0.433 MeV). The fractional difference in total cross section is about 2-5 % for higher-Z elements (Z ~ 70 to 90) and for energies 0.1-0.4 MeV. It becomes more (5-10 %) for energies greater than 0.4 MeV. For example the differences in the values of attenuation coefficient (total cross section) for Z = 26, 50, 74 and 82 in the energy scale 0.2-0.433 MeV from the two databases can be seen in Fig.2.1, where a good agreement is observed only for Z=26. It is worthwhile to mention here that the XCOM values are larger than the FFAST ones for tin, tungsten and lead in this energy range.

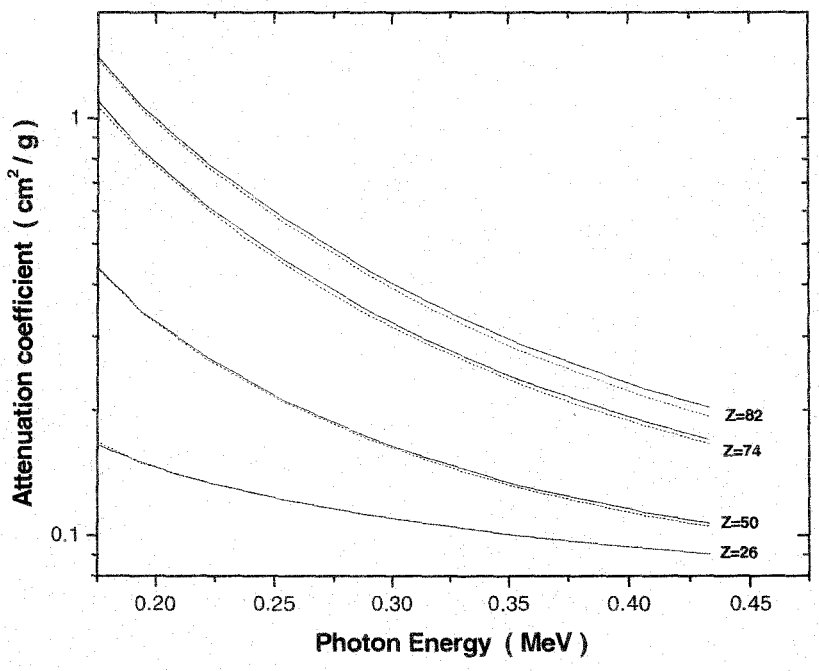

Fig.2.1. The theoretical predictions of attenuation coefficients (total cross sections). The solid and the dashed line represent the XCOM and FFAST values respectively.

Most of the earlier measurements were made with low resolution detectors like NaI. With the improvement in detector technology high resolution detectors with ever increasing efficiencies are available. As such, it is natural to repeat the attenuation coefficient measurement at all possible energies and for different materials using the latest technologies and adopting accurate methods. In a recent experiment in the energy

range 38-50 keV [123] the measured values of gold (Z = 79) were found to lie midway between the XCOM and FFAST values. At these energies XCOM and FFAST differ by about 4 %.

The accuracy of the value of attenuation coefficient of the scatterer has a direct impact on the accuracy of the measured value of elastic scattering cross section and hence on the observation of Delbrück scattering. Therefore, the values of attenuation coefficients of the scatterers used in the elastic scattering measurements were, precisely measured through a series of narrow beam experiments. Going a step further, measurements for few other targets and energies have also been made in an attempt to measure the photoelectric absorption cross sections of the targets.

2.2. Basic Criteria of a 'good geometry' for the experimental arrangement

In an experiment measuring attenuation coefficient or the total photon-atom cross section, one should be detecting only the un-deviated beam after the transmission of γ-ray beam through the absorber. The exponential nature of attenuation suggests that the photons interact via 'single' collision. These facts require that:

(a) the photons scattered by the absorber at a non-zero angle of scattering, however small the angle of scattering may be, must not be detected. In other words, the transmitted beam reaching the detector should consist only of un-deviated photons which come out from absorber without undergoing any type of interaction, and

(b) the photons suffering multiple scattering in the absorber should not be detected.

2.3. Experimental arrangements

Establishment of an experimental setup for detecting the attenuated beam of γ-rays in the forward direction, after transmission through an absorber, is well known and

straightforward. Deviations from the ideal good geometry lead to uncertainty in the measurements. For the sake of completeness, the various steps taken to fulfill the basic criteria mentioned in *Sec.* 1.2 and to minimize the uncertainty in the measurements have been discussed below.

2.3.1. Collimation of incident and the transmitted γ-ray beam and precaution against small angle scattering

In the experimental setup shown in Fig.2.2, the incident and the transmitted beam have been suitably collimated so as to reduce the number of photons reaching the detector which are scattered at very small angles. The γ-ray source S was placed in a lead block B_1 having 10-cm-deep conical bore. The block B_1 was then shielded on the sides and back by a minimum of 20-cm lead blocks. Collimator C_1 is a 23 cm thick iron block having a

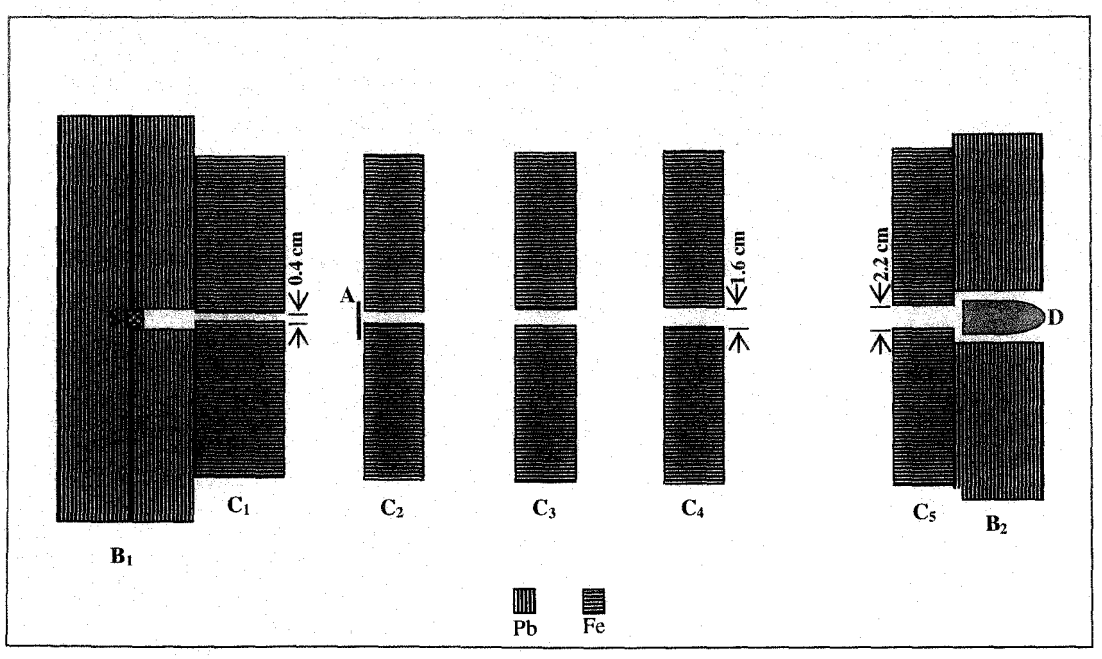

Fig.2.2. Schematic diagram showing the experimental arrangement used for the measurement of attenuation coefficients.

collimating bore of exit aperture 0.4 cm. Collimators C_2 to C_5, each 15-cm-thick iron block, produced a narrow beam collimation after transmission through the attenuator A. Collimators C_2 to C_4 have gradually increasing exit aperture, 1.6 cm. being the exit aperture of C_4. C_5 has a uniform cylindrical bore of diameter 2.2 cm. It prevents photons scattered in the shields and in the environs from reaching the detector D. These movable blocks were mounted on a rigid bench of iron and the optical alignment of the axis of bores was performed using a light source. The source to absorber and the absorber to detector distances were varied so as to reduce the value of the maximum angle of scattering θ_o (see Fig. 2.3) up to which the scattered photons can enter the detector but at the same time maintaining the solid angle subtended by the absorber at the centre of the detector at a lower possible value.

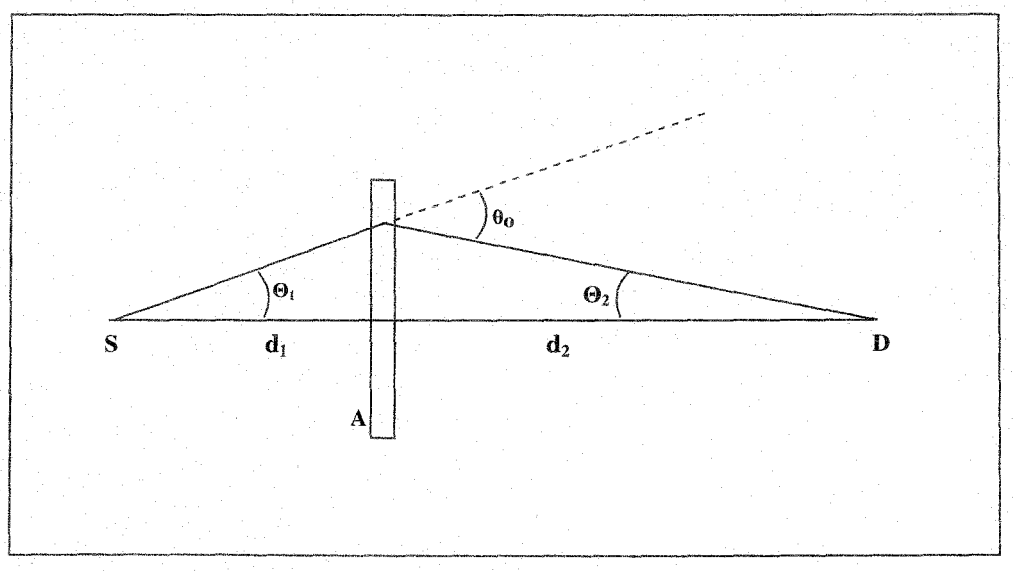

Fig.2.3. Diagram showing the maximum angle of scattering in the narrow beam collimation.

Keeping the source to detector distance fixed at 180 cm. we varied the positions of the absorber and the movable iron blocks so that the absorber was always in front of block C_2 whose entry aperture was 0.5 cm. From Fig. 2.3 one can see that

$$\theta_o = \theta_1 + \theta_2 \ ,$$

$$\theta_o \approx \frac{(D_A/2)}{d_1} + \frac{(D_A/2)}{d_2} \quad \text{and}$$

$$\omega_o = \frac{\pi (D_A/2)^2}{d_2^{\,2}} \tag{2.2}$$

where D_A (= 0.5 cm) is the diameter of the absorber exposed to the incident gamma radiation and ω_o is the maximum solid angle subtended by the absorber at the centre of the detector. Table 2.1 shows the variation of these angles θ_o and ω_o with the distances d_1 and d_2.

Table 2.1.

Variation of Maximum angle of scattering θ_o and Maximum solid angle of the scattering-cone ω_o

Geometry No.	Source to absorber distance d_1 (cm)	Absorber to detector distance d_2 (cm)	Maximum angle of scattering θ_o, of the scattered photon (minutes)	Maximum solid angle of the scattering-cone ω_o from absorber to the centre of detector (sr)
1	40	140	27.6	10.0×10^{-6}
2	55	125	22.5	12.6×10^{-6}
3	70	110	20	16.2×10^{-6}

Finally, we optimized an arrangement for which $\theta_o = 22.5'$ and the solid angle subtended by attenuator at the position of the detector was 12.6×10^{-6} sr. Smaller values of the solid angle ω_o is desirable for the set up as we wish to minimize the number of coherently or incoherently scattered photons from reaching the detector. Thus, in this geometry no photon scattered in the absorber at an angle greater than $22.5'$ could reach the detector. Similar experimental arrangements were adopted in [124]

2.3.2. Precaution against multiple scattering

If the thickness of the absorber is large, a significant number of multiply scattered photons from the absorber may reach the detector even when the primary incident beam is narrowly collimated. In order to reduce the number of such photons very thin absorbers are used. It has been observed that if the thickness (t) of the absorber is greater than one mean free path, multiple scattering could affect the measured value of attenuation coefficient (μ). Deterioration of the resolution of a detector with the increase in absorber thickness beyond 1/μ [125] is attributed not only to multiple scattering but also to bremsstrahlung from photoelectrons and Compton electrons produced in the target. In other investigations [126] on the effect of finite absorber dimension on γ-ray attenuation measurement it has been found that the effect is minimized if thin absorbers with $\mu t \ll 1$ are used. The change in full width at half maximum (FHWM) of the photo-peak, when an absorber with thickness t ($t > 1/\mu$) is placed in the path of the incident beam, shows the presence of multiple scattering. Absorbers having small thicknesses are to be chosen for which the FWHM of the photo-peak does not changed in the above process.

2.3.3. Requirements in the detector system

A coaxial high-purity germanium detector (HPGe) was procured from "Oxford Instruments", USA for the present set of measurements. The crystal characteristics were: diameter 57.7 mm; length 57 mm; hole-diameter 10.2 mm; hole-length 44.3 mm; germanium dead layer thickness, 600 μm (see Fig.2.4). The relative efficiency of the detector as measured by the manufacturer was 39.8%. The FHWM at 1.33 MeV was 1.77

keV and the peak to Compton ratio was 67.1. A "Tenelec" spectroscopic amplifier was used with 12 μs Gaussian peaking time. The amplified pulses were fed to the input of "Tenelec PCA3" pulse height analyzer fitted into an ISA slot of a Pentium-based computer. A high-quality "Assayer" data analysis software was used to control, acquire, store the spectrum in a binary data file and finally analyze the data. Further details of the detector are given in *Sec.* 3.3.3 of chapter 3.

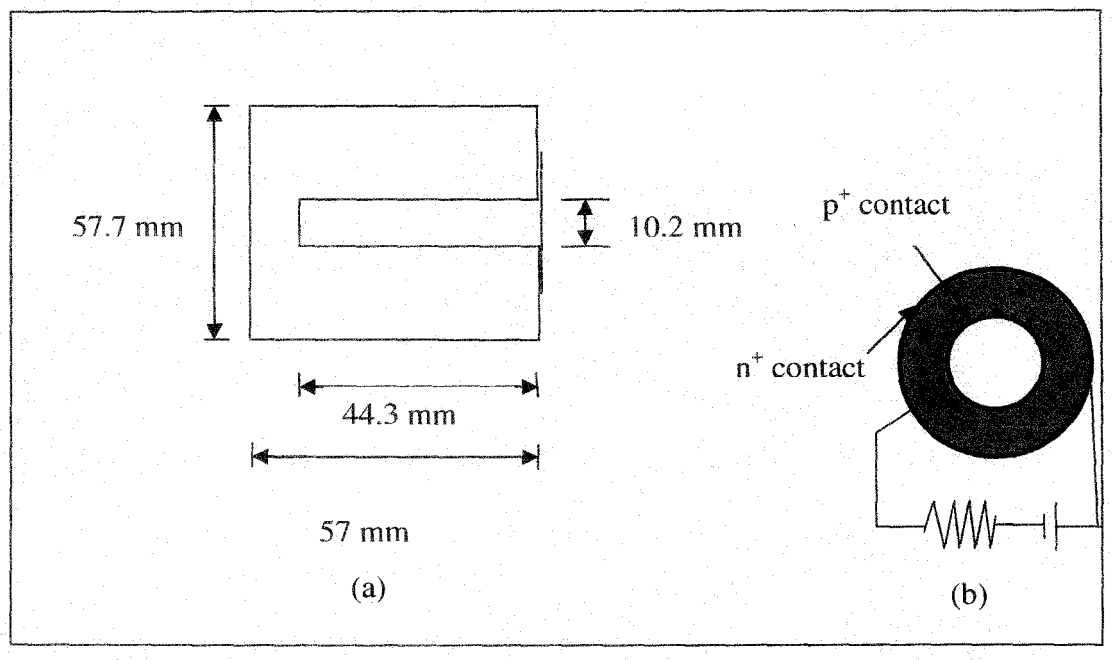

Fig.2.4. Schematic diagram showing (a) the HPGe crystal dimensions and (b) the fundamental biasing.

2.3.4. Gamma ray sources used in the measurements

A 200 mCi ^{65}Zn source (half-life = 243.8 days), procured from the Bhabha Atomic Research Center, Mumbai, India, was used as source of 1.115-MeV mono-energetic γ-ray photons. The source was encapsulated in a stainless steel capsule of dimension 1.0 cm diameter and 1.1 cm length whereas its active size was approximately 4mm. diameter x 3mm long. A weak ^{65}Zn reference source (20μC) was used in various

adjustment works like study of the drifting of photo-peak with respect to channel number as a function of time, calibration of energy channels and so on. Multiple-energy calibration of the whole window were performed with ^{137}Cs (Photon energy, ω = 0.662 MeV) and ^{60}Co (ω = 1.173 and 1.332 MeV). The strength of ^{60}Co source was approximately 10 mCi.

2.3.5. Absorbers used in the measurements

Solid tungsten and lead absorbers in the form of square (5 cm X 5 cm) sheets and of thicknesses of 1.93–12.35 g/cm2 and 1.135–3.80 g/cm2, respectively, were used. These 99.9995 % pure absorbers were procured from "Alfa Aeser", USA. Lead absorbers having thicknesses higher than 3.80 g/cm^2 were arranged locally and were 99.99 % pure. It is important that the target materials be thick enough to have a sufficient number of atomic targets yet be thin enough (much less than the mean free path of the photon, that is, $t \ll 1/\mu$) to avoid multiple scattering. Other absorbers used in the attenuation measurements, namely aluminum, iron and tin, were 99.99 % pure.

2.4. Experimental Method and Measurements

The absorption of γ-ray in matter is well known and is given by

$$I = I_0 \exp(-\mu t) \tag{2.3}$$

where μ is the linear attenuation coefficient, I and I_o are the intensities of transmitted and incident γ-rays respectively and t, the distance of matter traversed. If t is in g/cm^2 then μ in cm^2/g will be given by

$$\mu = \frac{\ln(I_o / I)}{t} \tag{2.4}$$

and the total photon cross section σ_{tot} is given by

$$\sigma_{tot}\ [barn/atom] = \mu\ [cm^2/g] \Big/ (N_A / A)\ \text{X}\ 10^{-24} \tag{2.5}$$

where N_A is Avogadro's number and A is the atomic weight of the absorber. In terms of transmission ratio R (=I / I_0) the attenuation coefficient is given by $\mu = (\ln(1/R))/t$. If a number of transmission measurements are done for a given absorber thickness at a particular γ-ray energy, the attenuation coefficient can be computed using the mean value of R and the average absorber thickness t. The standard deviation S_μ of the measured value of μ in terms of the standard deviations S_R of R and S_t of t is given by

$$S_\mu^{\,2} = \left(\frac{\partial \mu}{\partial R}\right)^2 S_R^{\,2} + \left(\frac{\partial \mu}{\partial t}\right)^2 S_t^{\,2} \tag{2.6}$$

If a mean value of μ is evaluated from μ's measured at n different thicknesses of the absorber, the standard deviation of the mean value can be written as

$$\bar{S}_\mu^{\,2} = \frac{1}{n^2}\sum_{i=1}^{n} S_{\mu,i}^{\,2} \tag{2.7}$$

where $S_{\mu,i}$ is the standard deviation of corresponding to i^{th} thickness of the absorber.

2.4.1. Procedure

As already stated the detector assembly was first tested for its stability in terms of drift in the photo peak and suitably calibrated. A perspex holder was used to place the absorber with its surface normal to the well collimated incident beam. Different transmitted data for the same sample were taken by exposing different portions of the surface so that error arising due to variation in thickness of the sample could be minimized. Corresponding to each acquisition of transmitted data, background counts were recorded for 2 to 3 hours by placing a 20 cm lead block in between C_4 and C_5 with (1) the source removed from its place (Bg-1) and (2) the source present in it place (Bg-2). The difference between count rates Bg-1 and Bg-2 were negligible which demonstrate the effectiveness of the shields and the collimators in preventing any rise in background in actual transmitted data. For each thickness of a sample, the spectra were acquired successively in the following order: background count (Bg-1), direct count or the count without absorber (DC), transmitted count or the count with absorber (TC), and

background count (Bg-2). The elapsed live times of the data acquisition varied from half an hour to several hours. As mentioned, Bg-1 ~ Bg-2.The time normalized background spectrum for each observation was subtracted from the transmitted spectrum and the direct spectrum. Selection of the region of interest of the photo-peak was done just within its FWHM by using the tool "ROI' of the analyzing software "Assayer" to obtain the integrated count N. The transmitted count rate N'=N/elapsed live time. Similarly, the direct count rate N_o' was obtained. Then, for each thickness the average of all N' and all N_o' were calculated as $\overline{N}'$ and $\overline{N}_o'$. As the distance between the source and detector and other geometrical factors remain the same, $I/I_o = \overline{N}'/\overline{N}_o'$.

The elapsed live time for a single photo-peak varied from 30 minutes to 8 hours so that the statistical errors were reduced to 0.1 to 0.3 %. For each sample, measurements were repeated for three or more thicknesses. Also, the systematic errors arising from geometry, absorber, source-size and background scattering effects have been reduced to an extent less than the statistical error.

2.4.2. Measurements

(A) Effect of solid angle on the attenuation coefficient measurements

A set of measurements of attenuation coefficient of lead at 1.115 MeV were done at the three different geometries (see Table 2.1.). The result showed that the influence of the solid angle was not significant.

(B) Effect of thickness of the absorber on the attenuation coefficient measurements

We carried out measurements of μ of lead at 1.115 MeV using the HPGe detector for various thicknesses keeping the geometry of the experimental same. As observed by other workers, we found that the effect of thickness on the measurements was negligible a long as the condition $\mu t \ll 1$ was satisfied. The FWHM of the photo peak was found to increase slightly when $t >> 1/\mu$.

(C) Attenuation coefficient Data

The attenuation data was taken in the geometry for which the source to absorber distance (d_1), the absorber to detector distance (d_2), the maximum angle of scattering of the scattered photon (θ_o), and the maximum solid angle of the scattering-cone from absorber to the centre of detector (ω_o) were 55 cm, 125 cm, 22.5 minutes and 12.6 $\times 10^{-6}$ sr respectively. The absorbers, mostly metals, were taken in the form of thin square sheet of approximate size 5cm x 5 cm. Three to six different thicknesses, satisfying $\mu t \langle\langle 1$, were chosen for each element. The average sample thickness was determined to an accuracy of 0.05 %. The samples taken were 99.99 % chemically pure. Mass attenuation coefficients of Al, Fe, Sn, W and Pb were measured at photon energies of 1.115, 1.173 and 1.332 MeV. . The overall accuracy in the result is of the order 1 %. Comparison of the measurements (present and earlier experimental data) with the XCOM predictions has been done in Table 2.2. A graphical comparison of the theoretical and the measured values of attenuation coefficients is presented in Fig. 2.5.

Table 2.2

Comparison of experimentally determined values of γ-ray attenuation coefficients with the XCOM predictions, all values are given in cm^2/g. The uncertainty in the last decimal place(s) is given within parenthesis

Element	Energy (MeV)	Present Measurements	Other Measurements	XCOM values Ref [119]
Al	1.115	0.0578(2)	0.0580(29)[a], 0.0583(2)[b]	0.05822
	1.173	0.0562(3)	0.0567(2)[b]	0.05676
	1.332	0.0530(3)	0.0531(2)[b]	0.05321

Table 2.2 (Continued)

Element	Energy (MeV)	Present Measurements	Other Measurements	XCOM values Ref [119]
Fe	1.115	0.0565(2)	0.0568(1)[b]	0.05671
	1.173	0.0548(3)	0.0557(1)[b]	0.05526
	1.332	0.0514(3)	0.0521(1)[b]	0.05181
Sn	1.115	0.0538(2)	0.05348(22)[c]	0.05432
	1.173	0.0526(2)	0.0528(5)[d]	0.05277
	1.332	0.0489(2)	0.0487(1)[d]	0.04924
W	1.115	0.0598(1)	0.0603(7)[e], 0.05964(28)[c]	0.06055
	1.173	0.0579(2)		0.05830
	1.332	0.0533(2)		0.05352
Pb	1.115	0.0638(1)	0.0658(10)[f], 0.06324(32)[c] 0.0640(1)[b], 0.0628(6)[e]	0.06444
	1.173	0.0612(2)	0.0615(1)[b], 0.0610(5)[g]	0.06175
	1.332	0.0554(2)	0.0557(1)[b], 0.0553(5)[g]	0.05616

[a] Umesh et al., Ref [127]

[b] Goswami and Chaudhuri, Ref [124]

[c] Conner et al., Ref [128]

[d] Hansen and Parthasaradhi, Ref [129]

[e] Murti et al., Ref [130]

[f] Umesh et al., Ref [131]

[g] Kane et al., Ref [132]

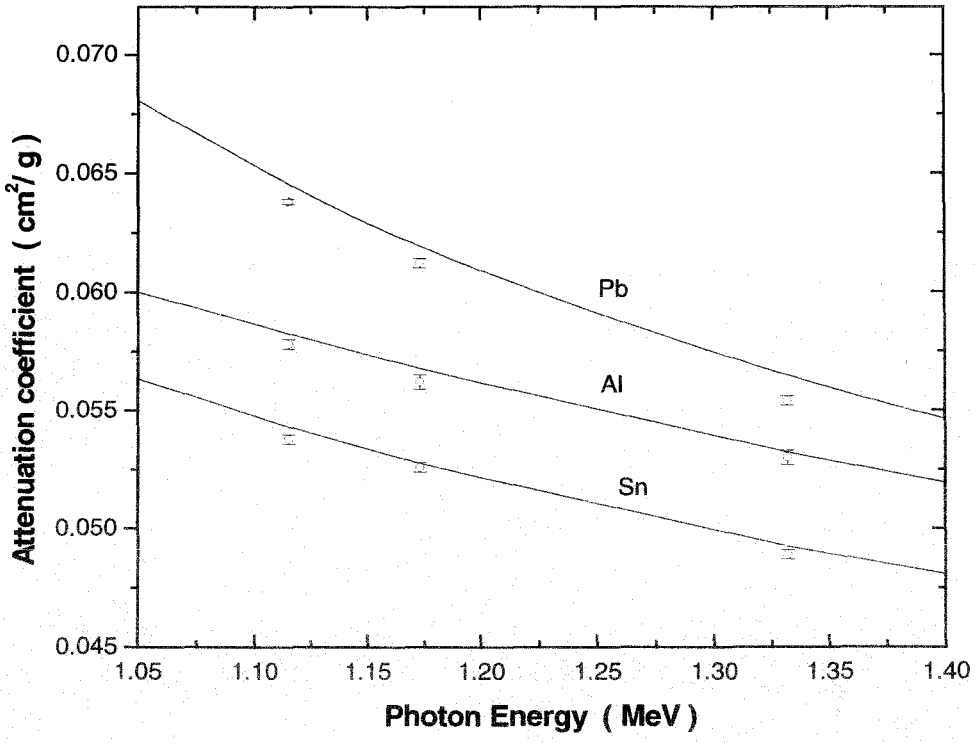

Fig.2.5.Measured attenuation coefficients of lead, aluminum and tin. The solid lines represent the XCOM predictions.

2.5. Evaluation of uncertainties in measurements

The total error in the measurement of attenuation coefficient of a sample at a given photon energy is evaluated by combining the standard deviation of the set of transmission ratios and the standard error of the thicknesses. Errors are evaluated following the eqns. (2.6) and (2.7) and are presented in Table 2.3.

The statistical errors were reduced, to an extent much lower than the systematic errors, by taking large numbers of counts for each set. The systematic errors arising from the following were taken into consideration:

(a) The photons scattered within the angle $\theta_0 = 22.5'$ and detected in the detector do not produce any significant error in the measurement. Through a calculation involving

integration of Compton and Rayleigh differential scattering cross sections within the limits $\theta = 0$ to $\theta = 22.5'$, we found that the contribution of scattering to the photo peak count is less than 0.3 %.

(b) The error arising out of multiple scattering was minimized by (i) choosing very thin samples as discussed in previous sections (ii) performing the experiment in the narrow beam geometry.

(c) The effect of energy degradation of primary photons due to Compton scattering within the volume of the radioactive source was not a source of error in the measurements as (i) the size of the source was very small (4mm. diameter x 3mm long), (ii) the detector had a better energy resolution (FWHM at 1.33 MeV was 1.77 keV).

Table 2.3.

A representative data showing the method of evaluation of results and the corresponding errors. Only the first significant figure in the fourth decimal place of the error is shown. (Absorber: lead; γ-ray energy: 1.115 MeV)

Average absorber thickness, t (g/cm^2)	Mean transmission ratio, R	$\frac{1}{R}$	$\mu = \frac{\ln(1/R)}{t}$ (cm^2/g)	Average μ (cm^2/g)	S_μ	$\bar{S}_\mu$
1.148	0.92874	1.0767	0.0641	0.0643	7	1
2.432	0.85504	1.1695	0.0642		3	
3.821	0.78186	1.2790	0.0643		2	
5.578	0.69821	1.4322	0.0643		1	
7.811	0.60469	1.6537	0.0644		1	
10.12	0.52116	1.9188	0.0644		1	

(d) Better energy resolution (FWHM at 1.33 MeV was 1.77 keV) of the HPGe detector ensured that the transmitted photo peak did not contain significant photon counts of other energies.

(e) A counting system loses some counts at high counting rates due to its finite resolving time. In the geometry followed in the present measurements, the dead time for all the acquired spectrum was nearly zero.

(f) The error due to background counts were minimized in the manner described in *Sec.* 2.4.1.

2.6. Photoelectric absorption cross sections derived from the measured mass attenuation coefficients

2.6.1. Introduction

In atomic photoabsorption an electron is ejected from an atom due to absorption of a photon. It is a vertex process in an external field in which the initial electron is discrete and the final electron state belongs to the continuum. Neglecting radiative corrections, the matrix element of the process ($\hbar = m = c = 1$) is

$$M = -e\,(2\pi)^{1/2}\,k^{-1/2}\int d^3r\;\psi_p^{*}\;\boldsymbol{\alpha}.\mathbf{e}\;e^{i\mathbf{k}.\mathbf{r}}\;\psi_B, \tag{2.8}$$

where **k** is the momentum and **e** is the polarization vector of the incoming photon, ψ_B is the electron wave function of the discrete (bound) state, and ψ_p is the electron wave function of the continuum state of momentum **p**. The differential cross section is obtained from

$$d\sigma = (2\pi)^{-2}\,|M|^2\;\delta(E)\,d^3p. \tag{2.9}$$

The bound wave function ψ_B is usually chosen in the hydrogen-like form and outgoing wave function ψ_p is taken as an appropriate solution of the Dirac equation in a pure Coulomb field. The details of theory of photoabsorption at high energies can be found in the review by Pratt *et al.* [133].

Several compilations of photoabsorption cross sections have been published. The tabulation by Storm and Israel [134] covering an energy range of 1 keV to 100 MeV is accurate within 2-3 %. Scofield [135] carried out calculations for individual subshells for all atoms Z=1 to 101 for photon energies 1 keV to 1.5 MeV and these photoabsorption cross sections are reported to be accurate within 0.1 %.

Hubbell *et al.* [118] prepared the complete tabulation by renormalizing the Scofield values in the energy region 1 to 1.5 MeV and they also extrapolated the Scofield cross sections up to 100 GeV by using an empirical formula developed by Pratt [136]. Photoabsorption cross sections can be found in the online database XCOM [119] which in the energy region 1 to 1.5 MeV is basically taken from [135].

Photoabsorption cross section are obtained experimentally, in the so called indirect method, by subtracting the cross sections of competing processes like Compton and Rayleigh scattering, pair production etc. from the measured total cross section. Thus, correctness of such measurement directly depends on the accuracy of theoretical predictions of competing processes. The direct method involves the determination of photoelectrons or x-ray intensity produced by the irradiation of the absorber with a known photon flux.

Photoabsorption is important not only from physics point of view but also due to its wide applications in other areas of research. Of the three processes Compton scattering, photoabsorption and pair production involved in the attenuation of a beam of photons in matter, Compton scattering is the most dominating contributor at energies near pair production threshold. For example, the attenuation in carbon (Z=6) at these energies is solely due to Compton scattering. As the atomic number (Z) of absorber increases contribution of photoabsorption to the total cross section also increases sharply. This can be seen in Fig.2.6 in which theoretical values of cross sections at a fixed photon-energy

of 1.115 MeV have been plotted against Z. Such behavior (Z^5 dependence) of photoabsorption is being explored in spectroscopic studies of astrophysical data, medical science and so on.

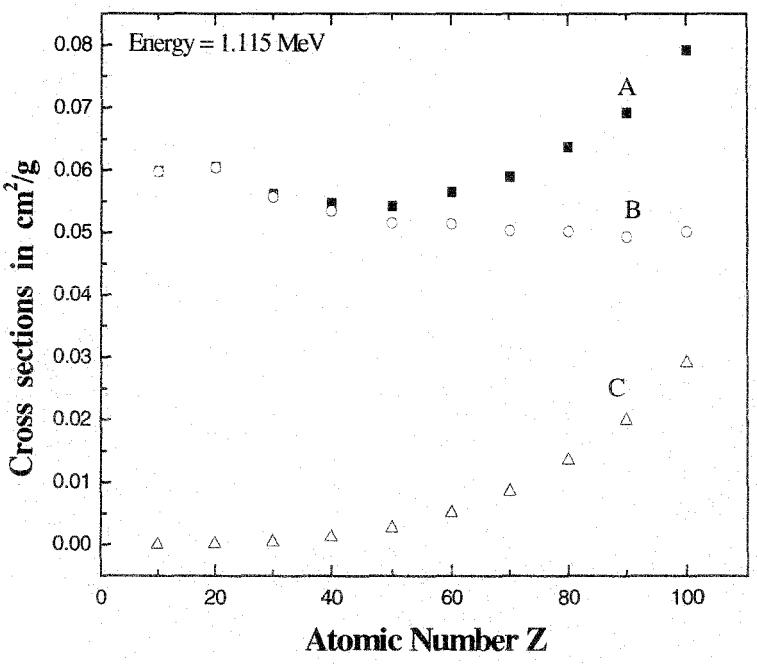

Fig.2.6. Theoretical cross sections of total (A), Compton (B) and photoabsorption (C) as a function of atomic number of the absorber.

2.6.2. Results

The measurements of photoabsorption cross sections using the HPGe detector at energies near the pair production threshold have been carried out for lead, tungsten and tin. For this an indirect method was followed in which photoabsorption cross section is obtained by subtracting other competing cross sections from the measured total cross section. The results are compared with the theoretical values of XCOM [119] and are presented in Table 2.4. The columns (1), (2) and (3) of Table 2.4 are theoretical cross sections [119] of Rayleigh scattering, Compton scattering and pair production

respectively. Column (4) is the sum of columns (1), (2) and (3). Experimental values of total cross sections, taken from the present measurements given in Table2.2, are shown in column (5). Theoretical cross sections [119] of photoabsorption are given in column (7).

Table 2.4

Measured photoabsorption cross sections near pair production threshold are obtained by subtracting column (4) from (5) and are depicted in column (6). All cross sections are expressed in barns/atom. Theoretical cross section in columns 1-3 and 7 are taken from XCOM

Atomic Number	Photon Energy (MeV)	(1) σ_{coh}	(2) σ_{incoh}	(3) κ_n	(4) [(1)+(2)+(3)]	(5) Measured total cross sections	(6) Photo-absorption cross section [(5)-(4)]	(7) Theoretical value of τ
82	1.115	0.8309	16.32	0.0133	17.16	21.95(3)	4.79(3)	5.013
	1.173	0.7525	15.91	0.0474	16.71	21.06(7)	4.39(7)	4.542
	1.332	0.5859	14.91	0.2604	15.76	19.06(7)	3.30(7)	3.564
74	1.115	0.6106	14.71	0.0104	15.33	18.26(3)	2.93(3)	3.154
	1.173	0.5526	14.35	0.0365	14.94	17.68(6)	2.74(6)	2.856
	1.332	0.4298	13.47	0.195	14.09	16.27(6)	2.18(6)	2.243
50	1.115	0.1995	9.975	0.0037	10.18	10.60(2)	0.42(2)	0.529
	1.173	0.1803	9.726	0.0128	9.919	10.37(4)	0.45(4)	0.481
	1.332	0.14	9.117	0.0664	9.324	9.64(4)	0.32(4)	0.381

The errors in the measured value of total cross sections are taken as the error of the derived photoabsorption cross section for a given energy and absorber (shown in the parentheses of column 6).

2.7. Discussions

The overall accuracy of the measured values of total cross section is less than 1 %. It is observed that the measured values of attenuation coefficients are in agreement with the theoretical values tabulated in XCOM [119]. Though the difference between the theory and the experiment is within 1.5 %, it is worthwhile to note that the most of the measured values of the total cross sections are consistently smaller than the XCOM predictions in this energy region (see Table 2.2).

The difference between the experimental and the theoretical values of photoabsorption cross section for lead has been found to vary up to 8 %. Obviously, such differences, cannot be attributed to the theoretical prediction of photoabsorption cross section in XCOM alone, as the sum of theoretical values of other competing processes have been subtracted from the measured total cross sections. The low Z absorbers ($Z<50$) have not been considered for the purpose as their photoabsorption cross sections are negligible compared to the total cross sections (τ is merely 0.5 % of total cross section in case for $Z=26$). The experimental values of photoabsorption cross sections, as in the case of total cross sections, are consistently smaller than the XCOM values.